ELSEVIER

International Journal of Solids and Structures 41 (2004) 4787–4807

INTERNATIONAL JOURNAL OF SOLIDS and STRUCTURES

www.elsevier.com/locate/ijsolstr

On the instantaneous energy release rate of the end-notch flexure adhesive joint specimen

K.S. Alfredsson *

Department of Engineering Science, University of Skövde, P.O. Box 408, S-541 28 Skövde, Sweden

Received 30 April 2003; received in revised form 11 March 2004
Available online 27 April 2004

Abstract

The energy release rate of the ENF adhesive joint specimen is derived. The resulting formula accounts for the presence of an adhesive layer with a possibly non-linear constitutive relation. The actual form of the constitutive relation need not to be known a priori. It is shown that measurements of both the applied load and the adhesive deformation at the crack tip are needed to determine the instantaneous value of the energy release rate. Experimental results show that the influence of the deformation of the adhesive layer can be substantial. The stability of the ENF-specimen is studied and a method to estimate the critical value of the crack length, accounting for the flexibility of the adhesive layer, is presented. In the analysis, the adherends are modelled as elastically deforming Euler–Bernoulli beams and the intermediate adhesive layer is modelled as a material surface transmitting shear stress between the adherends.

Keywords: Adhesive layer; Energy release rate; Shear fracture

1. Introduction

The end-notch flexure (ENF) geometry was introduced by Barrett and Foschi (1977) in a study of the fracture toughness of wood in shear. The concept was later extended to the closely related problems of delamination of composites (e.g. Carlsson et al., 1986) and shear testing of adhesive joints (cf. Chai, 1988). The ENF specimen (Fig. 1) consists of two adherends partially joined by an adhesive layer. The part of the specimen where the adherends are not joined by the adhesive can, in a macroscopic sense, be regarded as a crack. The end of this crack, i.e. where the adhesive starts, is in the sequel denoted the crack tip even though there might be no sharp (microscopic) crack. Due to the antisymmetric loading, the geometry provides essentially pure mode II conditions at the crack tip and it is well suited for shear testing of adhesives provided that the specimen is designed so that the adherends deform elastically. The specimen is used to determine the fracture energy, i.e. the energy needed to fracture a unit area of the adhesive layer. Provided that the adhesive

* Tel.: +46-500-448526; fax: +46-500-448599.
E-mail address: svante.alfredsson@ite.his.se (K.S. Alfredsson).

0020-7683/$ - see front matter © 2004 Elsevier Ltd. All rights reserved.
doi:10.1016/j.ijsolstr.2004.03.008

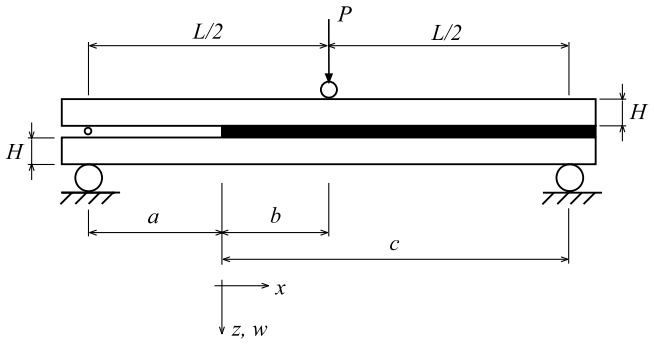

Fig. 1. Geometry of ENF-specimen. Dimensions used in example: $L = 1000$ mm, $H = W = 32.6$ mm, $t = 0.2$ mm (W = width, t = adhesive thickness). Initial crack length: $a = 350$ mm. Young's modulus of adherends: $E = 190$ GPa.

is loaded monotonically, this can be done indirectly by utilizing the energetic balance between the (apparent) elastic energy per unit area stored in the monotonically loaded adhesive at the crack tip, and the elastic energy released for a unit increase of the crack area. Measurement of the critical value of the energy release rate determines the fracture energy. A reliable method to experimentally obtain the energy release rate is thereby of vital importance. The objective of the present paper is to develop such a reliable method by deriving an explicit formula for the instantaneous energy release rate of the ENF-specimen.

Russel and Street (1982) present a simple formula for the energy release rate,

$$J_0 = \frac{9}{16}\frac{P^2a^2}{EW^2H^3} \tag{1}$$

It is based on the Euler–Bernoulli beam theory and does not account for the flexibility of the adhesive layer, i.e. corresponding to a rigid adhesive layer. Later, Chai and Mall (1988) use the same assumptions to derive a formula with extended validity to cases with a non-centrally applied load. Carlsson et al. (1986) derive an improved formula accounting also for shear deformation of the adherends, an important effect with adherends of composite materials. For specimens with slender metal adherends, however, this effect is negligible. Chai and Mall (1988) report a finite element analysis of a particular specimen configuration with a rigid adhesive layer. The analysis shows that Eq. (1) underestimates the energy release rate with only a few percent. Experiments on thin adhesive layers reported by Chai (1988) confirm this theoretical result, at least for loads which are only a fraction of the critical load for crack growth. For small loads, the adhesive deforms linearly elastically along the entire specimen. When testing tough engineering adhesives, however, the material at the crack tip experiences extensive non-linear deformation as the load is increased towards fracture. As shown in this paper, this gives large errors when using Eq. (1).

Several efforts to extend the applicability by accounting for the flexibility of the adhesive layer are reported in the literature, especially in the field of delamination of composites. Chatterjee (1991) uses both linear and non-linear models of the adhesive layer to obtain corrections to Eq. (1). Corleto and Hogan (1995) employ Timoshenko's beam theory and a generalized elastic foundation model for the adhesive layer. They conclude that the crack tip deformation is a critical factor in the evaluation of the energy release rate. This conclusion is supported by Ding and Kortschot (1999) who perform a similar analysis where only the crack tip region is modelled as an elastic foundation. All these reports indicate the importance of the flexibility of the adhesive layer. However, they are all limited to specific models for the adhesive layer and no general conclusions can be drawn regarding the corrections to Eq. (1).

In the present paper a formula for the energy release rate, accounting for the flexibility of the adhesive layer, is derived. The formula is based on the equations governing the deformation of the ENF-specimen

and requires no a priori knowledge of the constitutive relation of the adhesive layer. The formula consists of two dominating terms; the classical term in Eq. (1) and an additional term which is proportional to the product of the applied load and the crack tip deformation, cf. Eq. (36).

In the next section the governing equations are derived including the effect of a general non-linear relation between the shear deformation, v, of the adhesive layer and the shear stress, τ. In Section 3 the governing equations are used to derive an exact (within the theory used) formula for the energy release rate. At this point it is argued that the exact formula can be simplified. In order to verify this, an experiment is simulated using simplified constitutive models for the adhesive layer, cf. Fig. 4. The solution technique is briefly described in Section 4. In Section 5 the results of the simulations are used to obtain an approximate formula for the energy release rate and to establish conditions which must be fulfilled for the approximate formula to be valid. Experimental results are reported in Section 6. The final Section 7 is devoted to a study of the stability of the ENF-specimen.

2. Governing equations

In this section the equations governing the deformation of the ENF-specimen are derived. The geometry and the coordinate system used are shown in Fig. 1. Obviously, the test specimen is symmetric with respect to a line passing through the middle of the adhesive layer. Irrespective of details regarding the applied load and the support reactions, the loading is antisymmetric with respect to this geometrical symmetry line. Thus, the displacement field is essentially antisymmetric with respect to the line of symmetry. An anti-symmetric displacement field implies that the adhesive layer does not experience peel deformation. Strictly speaking, however, the conditions at the loading point and at the two supports are not antisymmetric. The effect of this deficiency is that peel stress occur near the loading point and at the right support. In these regions the peel stress can be of the same magnitude as the shear stress predicted by beam theory, cf. Salomonsson (2002). However, at the crack tip the peel stress is negligible. This is one reason why the ENF-specimen is suitable for shear testing of adhesive layers. Hence, peel deformation is neglected in this paper. Moreover, due to longitudinal straining of the adherends, the adhesive layer, beside the shear deformation, also experiences bending. As will be demonstrated below, this is most accentuated near the crack tip and the loading point. In general, the strains associated with bending of the adhesive layer are likely to be of a smaller magnitude than those associated with shear deformation, at least for situations where the adhesive material is weak as compared to the adherend material (cf. Klarbring, 1991; Schmidt, 2001). For the present case, the steel adherends are designed to deform within the elastic limit (cf. Alfredsson et al., 2003). Thus, the maximum strain related to bending of the adhesive layer is only about 0.1%. This is a very small strain as compared to the shear strain. The critical shear deformation, $v_c = 0.167$ mm, is of the same size as the adhesive thickness, $t = 0.2$ mm. Accordingly, effects of bending of the adhesive layer are neglected. The adhesive layer is thus assumed to deform in pure shear.

Consider now two points, one on each adherend, symmetrically located with respect to the middle of the adhesive layer, cf. Fig. 2. The longitudinal displacements of these points, in relation to a point located in the middle of the adhesive layer, are of equal magnitude but of opposite directions. In the following u denotes the longitudinal displacement in the positive/negative x-direction of the middle line of the lower/upper adherend. Both the longitudinal displacement, u, and the slope, w', contribute to the shear deformation of the adhesive. From the geometry shown in Fig. 2 it follows that, for small values of the slope ($|w'| \ll 1$), the shear deformation, v, of the adhesive layer is given by

$$v(x) = 2u(x) + Hw'(x) \tag{2}$$

where H is the height of each adherend. The constitutive relation for the adhesive is expressed in terms of the shear stress, τ, and the *total* shear deformation, v, of the adhesive layer. A constitutive relation for an

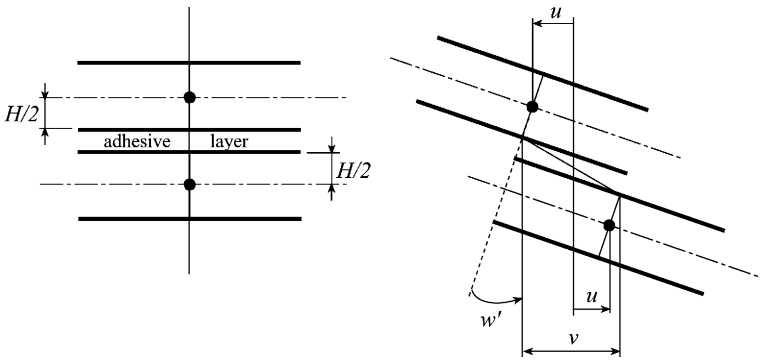

Fig. 2. Left: undeformed geometry; right: deformed geometry.

adhesive layer loaded in monotonically increasing shear is assumed to exist and to be valid for all points along the layer,

$$\tau = \tau(v) \tag{3}$$

The sectional forces and moments of the two adherends are antisymmetric with respect to the symmetry line, cf. Fig. 3. The normal forces on the two adherend cross sections are of equal magnitude but of opposite directions. Henceforth N denotes the tensional/compressive normal force of the lower/upper adherend. The shear forces and bending moments are equal for the two adherends. In the following V and M denote the shear forces and the bending moments of the adherends, respectively. The equilibrium equations read (cf. Alfredsson, 2003),

$$N'(x) = W\tau[v(x)], \quad V'(x) = 0 \tag{4a,b}$$

$$V(x) = M'(x) + \frac{1}{2}WH\tau[v(x)] \tag{4c}$$

where W is the width of the specimen. Assuming that the adherends deform elastically and according to the Euler–Bernoulli beam theory, the normal force and the bending moment are given by

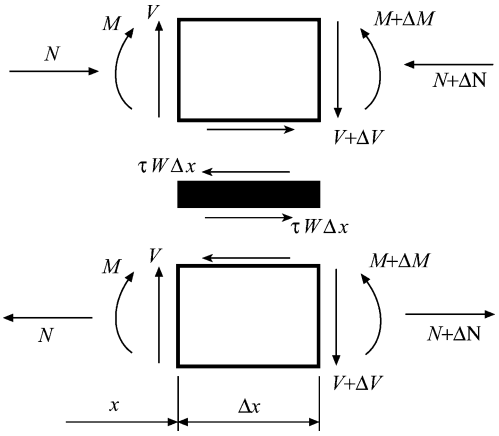

Fig. 3. Positive directions of adhesive stress and sectional loads.

$$N(x) = EWHu'(x), \quad M(x) = -\frac{EWH^3}{12}w''(x) \tag{5a,b}$$

where E is Young's modulus of the adherend material. Equations (5a,b) may be inserted into the differential equations (4a–c) whereby a system of ordinary differential equations in $u(x)$, $w(x)$ and $v(x)$ is obtained. These equations, complemented by the geometric relation (2) and the constitutive relation (3), state the mathematical problem. At a boundary, one of each in the three pairs of entities (N,u), (V,w) and (M,w') must be prescribed (cf. Alfredsson, 2003). For the present loading conditions it is advantageous to prescribe the normal forces, the bending moments and the shear forces at the adhesive boundaries,

$$N(0) = 0, \quad N(c) = 0 \tag{6a,b}$$

$$M(0) = Pa/4, \quad M(c) = 0 \tag{7a,b}$$

$$V(0) = P/4, \quad V(c) = -P/4 \tag{8a,b}$$

For a general constitutive relation (3) the governing equations given above constitute a non-linear boundary value problem. Its solution has a discontinuity in the shear force at the loading point. The normal force, the bending moment, the longitudinal displacement, the deflection and the slope, on the other hand, are continuous along the entire specimen. It follows from the differential Eq. (4b) and the boundary conditions (8a,b) that the shear force is constant along two portions of the specimen with a discontinuity at the point of load application,

$$V(x) = \begin{cases} +P/4 & \text{for } 0 \leqslant x < b \\ -P/4 & \text{for } b < x < c \end{cases} \tag{9}$$

Introducing Eq. (4c) into Eq. (9) results in the differential equation,

$$M'(x) + \frac{1}{2}WH\tau[v(x)] = \begin{cases} +P/4 & \text{for } 0 \leqslant x < b \\ -P/4 & \text{for } b < x < c \end{cases} \tag{10}$$

In order to obtain a boundary value problem which involves only the shear deformation, the longitudinal displacement and the deflection are eliminated from the governing equations. To this end, $\tau(v)$ is substituted from Eq. (4a) into Eq. (10). With N and M expressed in terms of the displacements u and w according to Eqs. (5a,b) the result is,

$$w'''(x) - \frac{6}{H}u''(x) = \begin{cases} -\dfrac{3P}{EWH^3} & \text{for } 0 \leqslant x < b \\ +\dfrac{3P}{EWH^3} & \text{for } b < x < c \end{cases} \tag{11}$$

By differentiating Eq. (2) twice and using Eq. (11), a relation between the second derivatives of u and v is obtained,

$$8u''(x) = \begin{cases} v''(x) + \dfrac{3P}{EWH^2} & \text{for } 0 \leqslant x < b \\ v''(x) - \dfrac{3P}{EWH^2} & \text{for } b < x < c \end{cases} \tag{12}$$

With the second derivative of u from Eq. (12) inserted into the equation obtained by inserting Eq. (5a) into Eq. (4a), a resulting differential equation is found,

$$EHv''(x) = \begin{cases} 8\{\tau[v(x)] - \bar{\tau}\} & \text{for } 0 \leqslant x < b \\ 8\{\tau[v(x)] + \bar{\tau}\} & \text{for } b < x < c \end{cases} \tag{13}$$

where $\bar{\tau}$ is identified as the shear stress as predicted by Jouravski's theory for shear stresses in solid beam sections (e.g. Beer et al., 2002),

$$\bar{\tau} = \frac{3}{8}\frac{P}{WH} \tag{14}$$

According to Eq. (2) and the discussion following Eq. (8), both v and v' are continuous along the entire specimen. The remaining boundary conditions (6a,b) and (7a,b) transform to

$$v'(0) = -8\frac{\bar{\tau}a}{EH}, \quad v'(c) = 0 \tag{15a,b}$$

Equations (13) and (15a,b) show the non-linear boundary value problem in a form where only the shear deformation appears. These equations are used in the following to derive a formula for the energy release rate, cf. Eqs. (22) and (36).

The deflection, $w(x)$, of the specimen is determined from integration of Eq. (5b), where the bending moment in the adherends is given by

$$M(x) = \begin{cases} \frac{1}{4}P(x+a) - \frac{1}{2}HN(x) & \text{for } -a \leqslant x \leqslant b \\ \frac{1}{4}P(c-x) - \frac{1}{2}HN(x) & \text{for } b \leqslant x \leqslant c \end{cases} \tag{16}$$

Here, the normal force in the adherends is given by

$$N(x) = W\int_0^x \tau[v(\tilde{x})]\,\mathrm{d}\tilde{x} \tag{17}$$

which follows from Eqs. (4a) and (6a).

3. Energetic balance

The shear stress distribution in the ENF-specimen is non-uniform. This makes it virtually impossible to use the test specimen for a direct [1] measurement of the adhesive constitutive relation, $\tau(v)$. The specimen is, however, recognized to be well suited for measuring the fracture energy, i.e. the ultimate value of the *energy release rate*,

$$J = \int_0^{v(0)} \tau(\tilde{v})\,\mathrm{d}\tilde{v} \tag{18}$$

For an ENF-specimen with a *rigid* adhesive layer (e.g. Chai and Mall, 1988), the energy release rate is given by Eq. (1). This equation is frequently used to deduce the fracture energy from experiments. However, the presence of a compliant adhesive layer affects the value of J. The equations governing the deformation of the specimen are hence used to obtain an expression for J which includes the effect of the adhesive compliance. For this purpose, a technique developed by Olsson and Stigh (1989), to derive the energy release rate of the DCB-specimen, is followed. Thus, Eq. (13) is multiplied by $v'(x)$ and integrated from the crack tip to the loading point,

$$EH\int_0^b v''(x)v'(x)\,\mathrm{d}x = 8\int_0^b \{\tau[v(x)] - \bar{\tau}\}v'(x)\,\mathrm{d}x \tag{19}$$

[1] Alfredsson et al. (2003) describe an *inverse* method to obtain the adhesive constitutive relation.

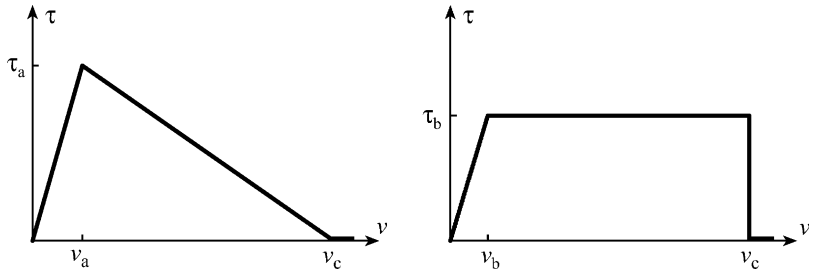

Fig. 4. Simplified constitutive relations for adhesive layer. Left: sawtooth model. Right: ideal-plastic model.

The integral on the left hand side is evaluated directly and the integrating variable of the integral on the right hand side is shifted from x to v,

$$\frac{EH}{2}\left[\{v'(x)\}^2\right]_0^b = 8\int_{v(0)}^{v(b)}\{\tau(v)-\bar{\tau}\}\,\mathrm{d}v \tag{20}$$

Evaluating the integral for the second term of the right hand side it follows that,

$$\int_{v(b)}^{v(0)}\tau(v)\,\mathrm{d}v = \frac{EH}{16}\left[\{v'(x)\}^2\right]_b^0 + \bar{\tau}\{v(0)-v(b)\} \tag{21}$$

Introducing the boundary condition (15a) and inserting $\bar{\tau}$ from Eq. (14), the energy release rate defined by Eq. (18) takes the form,

$$J = \frac{9}{16}\frac{P^2a^2}{EW^2H^3} - \frac{EH}{16}\{v'(b)\}^2 + \frac{3}{8}\frac{P}{WH}\{v(0)-v(b)\} + \int_0^{v(b)}\tau(v)\,\mathrm{d}v \tag{22}$$

This formula for J is exact within the theory applied here. The first term is obviously equal to J_0 which is the energy release rate for the case of a rigid adhesive layer, cf. Eq. (1). The other terms represent corrections of J_0 that account for the flexibility of the adhesive layer. The size of these terms depend on the specific case. In some cases the first term may suffice. However, it is noted from Eq. (22) that, in the general case, the force, P, the adhesive shear deformation at the crack tip, $v(0)$, and at the loading point, $v(b)$, and $v'(b)$ must be measured. Moreover, in order to evaluate the last term in Eq. (22), $\tau(v)$ must be known in advance. However, if the distance between the crack tip and the loading point, b, is large enough, the shear deformation at the loading point, $v(b)$, is much smaller than the shear deformation at the crack tip, $v(0)$. The last two terms in Eq. (22) can then be neglected. This also means that $\tau(v)$ need not to be known in advance. By differentiation of Eq. (2) it is shown that $|v'|$ is twice the tensile/compressive strain in the adherends at the upper/lower interface. The second term of Eq. (22) could thus be determined from measurements of the strains in the adherends at the loading point. As demonstrated in Section 5, however, this term can be adequately approximated without the need of any strain measurements. In order to justify the approximations discussed here, the development of the deformation field, $v(x)$, is first simulated for two simplified constitutive models, cf. Fig. 4. The simulations are used to motivate an approximate formula for J containing measurable quantities.

4. Simulation of an experiment — solution procedure

In order to study the size of the terms in Eq. (22), an experiment is simulated using simple $\tau(v)$ relations, cf. Fig. 4. A simple mathematical form of a typical constitutive relation is the "sawtooth model", cf. the left

part of Fig. 4, used by e.g. Ungsuwarungsri and Knauss (1987), Stigh (1988), Mi et al. (1998) and Zou et al. (2003). In a numerical simulation, such a piecewise linear relation catches the important features without leading to too complicated equations. Besides the sawtooth model, simulations with the "ideal-plastic" model are performed. In contrast to the sawtooth model, this model loses its load bearing capacity abruptly, cf. the right part of Fig. 4. Thus, the two adhesive models in Fig. 4 are fundamentally different, which gives substance to the conclusions drawn from the simulations. A solution technique is developed below, where the present problem is worked out by solving *linear* equations.

It should be noted that the constitutive relations discussed here, cf. Eq. (3), are relations between the stress acting at the adherend/adhesive interface and the *total* deformation of the adhesive *layer*. Theoretically, this corresponds to averaging over a Representative Volume Element containing a number of microcracks (e.g. Xia and Hutchinson, 1994). With this level of modelling, the precise micromechanics of deformation and fracture in the adhesive layer is not modelled. Instead it is manifested in the form of the relation $\tau(v)$. A typical constitutive relation for an adhesive layer has an initial linear part followed by a part where the stiffness decreases until a maximum is reached. The maximum is followed by a strain-softening part where the load carrying capacity is reduced to zero. This has been found experimentally for adhesive layers loaded in peel (Stigh and Andersson, 2000; Sørensen, 2002; Andersson and Stigh, 2003) and for adhesive layers loaded in shear (Wernersson and Gustafsson, 1987; Alfredsson et al., 2003). The strain–softening is most likely due to the formation of microcracks and voids in the interior of the adhesive layer, eventually leading to macroscopic fracture of the adhesive layer, i.e. cohesive fracture. Another source of strain softening is adhesive fracture, i.e. fracture at the adhesive/adherend interface.

The numerical data used in the simulations are based on the experimental results presented in Section 6. Thus, the fracture energy and the critical shear deformation are $J_c = 3420$ J/m^2 and $v_c = 0.167$ mm, respectively. The initial stiffness of the adhesive layer is $k = 4300$ GN/m^3. For the *sawtooth model*, $k = \tau_a/v_a$ and $\tau_a = 2J_c/v_c$. For the *ideal-plastic model*, $k = \tau_b/v_b$ and $\tau_b = kv_c(1 - \sqrt{1 - 2J_c/(kv_c^2)})$. This gives the numerical values of the model parameters: $\tau_a = 41.0$ MPa, $v_a = 9.53$ μm, $\tau_b = 20.8$ MPa and $v_b = 4.83$ μm.

The solution is divided into three parts: First, a linear elastic solution is obtained, corresponding to an applied load small enough to ensure that the adhesive layer is linear elastic throughout. Increasing the load further results in initiation and growth of a process zone at the crack tip. This is the second part of the solution, where the global stiffness is gradually diminishing. The third part corresponds to crack growth. In this part, the applied load and the size of the process zone decrease as the deformation at the crack tip is increased beyond the critical value.

4.1. Solution for a linear elastic adhesive

For moderate magnitudes of the applied load, the shear deformation is small at all points of the adhesive layer. The constitutive relation is then given by $\tau(v) = kv$, and Eq. (13) results in a linear differential equation of second order,

$$v''(x) - \kappa^2 v(x) = \begin{cases} -\kappa^2\bar{\tau}/k & \text{for } 0 \leqslant x \leqslant b \\ +\kappa^2\bar{\tau}/k & \text{for } b \leqslant x \leqslant c \end{cases} \tag{23}$$

where $\kappa \equiv \sqrt{8k/EH}$ constitutes the inverse of a length scale of the solution. The general solution to this equation is given by

$$v(x) = \begin{cases} A_1 e^{\kappa x} + A_2 e^{-\kappa x} + \bar{\tau}/k & \text{for } 0 \leqslant x \leqslant b \\ A_3 e^{\kappa x} + A_4 e^{-\kappa x} - \bar{\tau}/k & \text{for } b \leqslant x \leqslant c \end{cases} \tag{24}$$

The integration constants A_1, A_2, A_3 and A_4 are determined by the boundary conditions (15a,b) and the requirement on continuity of v and v' at $x = b$.

4.2. Growth of process zone

As the displacement of the loading point is increased, the adhesive deformation, $v(0)$, at the crack tip, reaches the proportionality limit, v_a or v_b, cf. Fig. 4. When the displacement of the loading point is increased further, a process zone starts to develop at the crack tip. The length of the process zone is denoted by d. Thus, the process zone occupies the region ahead of the crack tip ($0 \leqslant x \leqslant d$). In the following analysis it is assumed that the process zone does not include the loading point, i.e. $d < b$, cf. Fig. 1.

For the *sawtooth model*, the deformation inside the process zone is governed by $\tau(v) = \bar{k}(v_c - v)$, where $\bar{k} = \tau_a/(v_c - v_a)$. Insertion into Eq. (13) yields a linear differential equation of second order,

$$v''(x) + \bar{\kappa}^2 v(x) = \bar{\kappa}^2(v_c - \bar{\tau}/\bar{k}) \quad \text{for } 0 \leqslant x \leqslant d \tag{25}$$

where $\bar{\kappa} \equiv \sqrt{8\bar{k}/EH}$. The general solution is given by

$$v(x) = \begin{cases} B_1 \sin(\bar{\kappa}x) + B_2 \cos(\bar{\kappa}x) + v_c - \bar{\tau}/\bar{k} & \text{for } 0 \leqslant x \leqslant d \\ B_3 e^{\kappa x} + B_4 e^{-\kappa x} + \bar{\tau}/k & \text{for } d \leqslant x \leqslant b \\ B_5 e^{\kappa x} + B_6 e^{-\kappa x} - \bar{\tau}/k & \text{for } b \leqslant x \leqslant c \end{cases} \tag{26}$$

For the *ideal-plastic model*, $\tau(v) = \tau_b$ in the process zone. Insertion into Eq. (13) yields,

$$v''(x) = \frac{\tau_b - \bar{\tau}}{k}\kappa^2 \quad \text{for } 0 \leqslant x \leqslant d \tag{27}$$

The general solution is given by

$$v(x) = \begin{cases} C_1 \frac{x}{L} + C_2 + \frac{1}{2}\frac{\tau_b - \bar{\tau}}{k}\kappa^2 x^2 & \text{for } 0 \leqslant x \leqslant d \\ C_3 e^{\kappa x} + C_4 e^{-\kappa x} + \bar{\tau}/k & \text{for } d \leqslant x \leqslant b \\ C_5 e^{\kappa x} + C_6 e^{-\kappa x} - \bar{\tau}/k & \text{for } b \leqslant x \leqslant c \end{cases} \tag{28}$$

The non-linear problems are now solved by utilizing a technique similar to the one presented by Stigh (1988) in a crack growth analysis of a DCB-specimen. Hence, the length of the process zone, d, is used as an independent variable. The six constants of integration and the applied load, represented by $\bar{\tau}$, are to be determined. Thus, seven equations are needed. Two equations are given by the boundary conditions (15a,b). Four more equations are given by the fact that both v and v' must be continuous at $x = d$ and at $x = b$. The final seventh equation is provided by the knowledge of the level of deformation at the right end of the process zone: $v(d) = v_a$ for the sawtooth model and $v(d) = v_b$ for the ideal-plastic model. It is noted that the resulting system of equations is linear in the integration constants (B_i or C_i) and $\bar{\tau}$. For a given value of d, they are easily determined by solving the linear system of equations. Thus, each value of d corresponds to a force, represented by $\bar{\tau}$, and a distribution of shear deformation, given by the constants $B_{1\text{–}6}$ or $C_{1\text{–}6}$. By analysing an increasing sequence of d, the load-deformation history is obtained, i.e. $\bar{\tau}[v(0)]$.

As the size of the process zone, d, is increased, the adhesive deformation at the crack tip eventually reaches the critical value, i.e. $v(0) = v_c$. The corresponding size of the process zone, d_c, is, for the *sawtooth model*, determined from Eq. (26) by $B_2 = \bar{\tau}/\bar{k}$. For $e^{-\kappa b} \ll 1$, the resulting equation is approximately given by

$$f_1(d) + f_2(d) = 0 \tag{29a}$$

where

$$f_1(d) = \kappa[kv_a + \bar{k}(v_a - v_c)] + 2\bar{k}\kappa(v_c - v_a)e^{\kappa(d-b)} \tag{29b}$$

$$f_2(d) = k\bar{\kappa}[v_a(\kappa a + 1) - v_c]\sin(\bar{\kappa}d) + k[\bar{\kappa}^2 a(v_a - v_c) - \kappa v_a]\cos(\bar{\kappa}d) \tag{29c}$$

For the *ideal-plastic model*, the critical size of the process zone, d_c, is determined from Eq. (28) by $C_2 = v_c$, or approximately for $e^{-\kappa b} \ll 1$,

$$\frac{\kappa[\kappa a d(\kappa d/2+1)+a+d]+1+(\kappa^2 d^2-2)e^{\kappa(d-b)}}{\kappa(a+d)+1-2e^{\kappa(d-b)}} - \frac{v_c}{v_b} = 0 \tag{30}$$

It should be noted that the approximate equations (29) and (30) provides excellent estimates of d_c when $e^{-\kappa b} \ll 1$.

4.3. Crack growth

As the displacement of the loading point is increased further, the shear deformation at the initial crack tip exceeds the critical value, v_c. This phase of the loading sequence corresponds to crack growth. In the mathematical analysis of crack growth, the crack length a is increased, and a new size of the process zone, d, is calculated using Eq. (29) or (30). Once the size of the process zone is known, the shear stress distribution and the load level is obtained similarly as in the previous analysis for growth of process zone, i.e. by solving a linear system of equations. It can be noted that, as the crack propagates, the size of the process zone decreases slightly from the value, d_c, prevailing at the start of crack growth. The same effect is observed by Stigh (1988) in analysing the DCB-specimen under similar conditions. This effect appears to be a general feature of the use of a stress-deformation relation to model an adhesive layer.

5. Approximate formula for the energy release rate

The objective of the present section is to simplify the general form of the instantaneous energy release rate, cf. Eq. (22), and to establish the conditions that must be fulfilled for an approximate formula to be valid. To be more specific, the condition to be fulfilled is that the distance, b, between the crack tip and the loading point is large enough so that the adhesive deformation at the loading point is negligibly small. In order to quantify this condition, an experiment is simulated using the technique described in the previous section. The development of the deformation field is studied, as the deformation at the crack tip increases from zero towards and beyond fracture. Conclusions regarding the size of the different terms in Eq. (22) are drawn from the results of the simulations.

Fig. 5 shows results for the case of a *linear elastic adhesive*. The dotted curve depicts the shear stress distribution for a specimen containing no crack ($a = 0$). In the present case the test specimen is long in a relative sense, i.e. the value of κL is large. Under these circumstances, the shear stress is close to $\bar{\tau}$, predicted by Jouravski's theory, except for a narrow region in the vicinity of the loading point where a change of sign takes place. A shorter test specimen (not shown here), exhibits a more shallow shear stress distribution with maximum values lower than the ones predicted by Jouravski's theory. The other curves in Fig. 5 represent the shear stress distribution when a crack is introduced. It is seen that the shear stress distribution some distance from the crack tip remains practically the same as when no crack is present. This is true as long as the distance between the crack tip and the loading point, b, is 'long enough'. For a linear elastic adhesive, b can be regarded as long if $\kappa b \geqslant 5$. If this condition is met, the solution described in Section 4.1 gives approximate values of the deformation at the crack tip and at the loading point,

$$\tau(0) = kv(0) \simeq \bar{\tau}(\kappa a + 1) \equiv \tau_{ce} \tag{31a}$$

$$v(0) \gg v(b) \simeq 0, \quad v'(b) \simeq -\frac{\bar{\tau}\kappa}{k} = -\frac{P}{W}\sqrt{\frac{9}{8}\frac{1}{EkH^3}} \tag{31b,c}$$

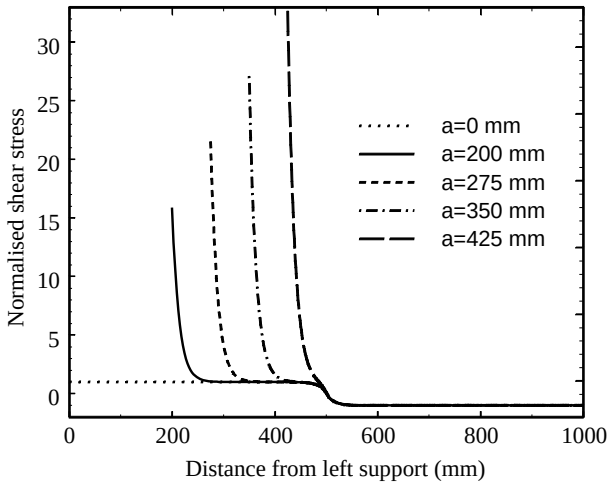

Fig. 5. Normalised shear stress distribution, $\tau/\bar{\tau}$, in a linear elastic adhesive layer.

It can be noted that $\kappa b \simeq 6$ for the curve in Fig. 5 corresponding to the crack length $a = 425$ mm. The difference between τ_{ce} and $\tau(0)$ is less than 0.03% for this case. As seen in Fig. 5, τ_{ce} is generally substantially larger than $\bar{\tau}$. The energy release rate, for the case of a linear elastic adhesive, is found by inserting Eqs. (31a–c) into Eq. (22), or directly by inserting Eq. (31a) into the definition (18),

$$J_{\text{lin}} = J_0\left(1 + \frac{1}{\kappa a}\right)^2 \tag{32}$$

where J_0 is the energy release rate for the case of a rigid adhesive, cf. Eq. (1). It is thus found that the presence of a linear elastic adhesive gives an increase of the energy release rate. The size of this effect is only governed by the value of κa, provided, of course, that $\kappa b \geqslant 5$.

The attention is now directed to the *non-linear adhesive* models depicted in Fig. 4. A process zone develops in front of the crack tip. For the present case, both from the solution of the exact equations and the approximate equations (29) and (30), the calculated values of the critical size of the process zone are $d_c = 81$ mm for the sawtooth model and $d_c = 115$ mm for the ideal-plastic model. Thus, the size of the process zone is about three times the height of the adherends and several hundred times the adhesive thickness ($t = 0.2$ mm). Fig. 6a shows the shear stress distribution in the adhesive layer when the deformation at the crack tip has reached the critical value, i.e. at the onset of crack growth. The dotted line depicts the stress distribution for the case of no crack ($a = 0$) at the same load level. It is seen that the adhesive deformation at the loading point is practically unaffected by the presence of the crack and the process zone. Fig. 6b shows the shear stress distribution when the crack has propagated to a length of $a = 380$ mm. It is seen that, for both the sawtooth and the ideal-plastic models, the shear stress at the loading point differs somewhat from the "no crack" solution (dotted curve). Numerical simulations show that, as long as the distance between the crack tip and the loading point is large, i.e. if κb is large, Eqs. (31b,c) are good approximations also in the non-linear case. The presence of a process zone means that, as compared to the linear elastic case, a larger value of κb is needed in order to obtain good approximations from Eqs. (31b,c). For a non-linear adhesive it is not straightforward to give an explicit formula for the required value of b. This value depends both on the elastic properties of the specimen (through κ) and on the size of the process zone. The size of the process zone is, in turn, dependent of the constitutive relation

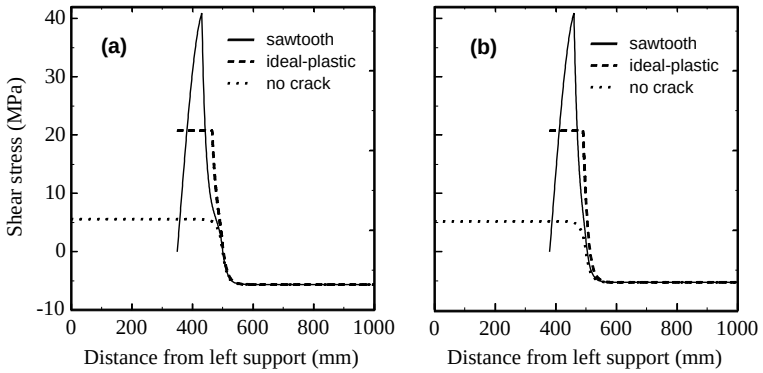

Fig. 6. (a) Shear stress distribution in adhesive layer at the onset of crack propagation. (b) Shear stress distribution in adhesive layer when the crack has propagated 30 mm.

and the geometry of the specimen. For the present adhesive, it is found by numerical simulations that the approximations in Eq. (31b,c) give good accuracy, provided that $\kappa b \geqslant 10$.

We are now in a position to simplify the general expression for the energy release rate, cf. Eq. (22). As described above, the conditions at the loading point is approximated with good accuracy according to Eqs. (31b,c), provided that $\kappa b \geqslant 10$. The second term in Eq. (22) is approximated using $v'(b)$ from Eq. (31c). The fourth term in Eq. (22) is discarded, since $v(b)$ can be neglected as compared to $v(0)$ according to Eq. (31b). The last term in Eq. (22) is discarded for the same reason. Thus, an approximate formula for the energy release rate with a non-linear adhesive reads

$$J_{\text{app}} = J_0 + \frac{3}{8}\frac{P\,v(0)}{WH} - \frac{9}{128}\frac{P^2}{kW^2H^2} \tag{33}$$

This formula for the energy release rate is valid not only prior to fracture, but also during crack growth. The coordinate system used in the derivation of Eq. (22) indicates that, during crack growth, $v(0)$ should be measured at the instantaneous position of the crack tip. However, it is possible to avoid this by utilizing the fact that the strain at the former adherend/adhesive interfaces is known. To this end, it is first noted that the shear deformation at the instantaneous crack tip, $v(0)$, is related to the shear deformation at the initial crack tip, v_{in}, through

$$v(0) = v_{\text{in}} + \int_{-(a-a_{\text{in}})}^{0} v'(x)\,\mathrm{d}x \tag{34a}$$

It follows from Eq. (2) and Fig. 2 that $v'/2$ is the negative/positive of the longitudinal strain at the upper/lower adherend/adhesive interface, i.e.

$$v'(x) = -\frac{12M(x)}{EWH^2} \quad \text{for} \quad -a \leqslant x \leqslant 0 \tag{34b}$$

Using the distribution of the bending moment, $M(x)$, from Eq. (16), inserting Eq. (34b) into Eq. (34a), and integrating, yields

$$v(0) = v_{\text{in}} - \frac{3}{2}\frac{P}{EWH^2}(a^2 - a_{\text{in}}^2) \tag{35}$$

With this relation inserted into Eq. (33) it follows,

$$J_{\text{app}} = J_{0\text{in}} + J_1 - J_2 \tag{36a}$$

where

$$J_{0\mathrm{in}} = \frac{9}{16}\frac{P^2 a_{\mathrm{in}}^2}{EW^2H^3}, \quad J_1 = \frac{3}{8}\frac{P v_{\mathrm{in}}}{WH}, \quad J_2 = \frac{9}{128}\frac{P^2}{kW^2H^2} \tag{36b,c,d}$$

This is the key equation of the present paper. The only entities in the formula varying during a test are the applied load, P, and the adhesive shear deformation at the initial position of the crack tip, v_{in}. They can both be measured. All other entities are either geometrical data (a, W, H) or material constants (E, k).

The adhesive models treated here are based on a unique constitutive relation, $\tau(v)$, valid also during crack growth. This means that the fracture energy, J_c, is constant during crack growth, cf. Eq. (18). The solid curves of Fig. 7 show the progress of J, for the two adhesive models, as calculated from the approximate formula (36). Prior to crack growth, the approximate values, J_{app}, are in excellent agreement with the exact value, J, given by the calculated crack tip deformation and the definition (18). It is seen that, during crack growth, J_{app} deviates somewhat from the exact constant fracture energy, J_c, especially for the ideal-plastic model. This is due to the non-zero adhesive deformation at the loading point, cf. Fig. 6b. The discrepancy is, however, less than 0.1% at the start of crack growth and less than 0.7% when the crack has propagated 30 mm. This indicates that, for the present geometry, the approximate formula (36) is accurate enough to give a good estimate of the energy release rate until the crack has grown to a length of 380 mm. For a specimen with a larger distance between the crack tip and the loading point, the error is even smaller. The contributions from the different terms in Eq. (36) are also shown in Fig. 7. These results indicate that $J_{0\mathrm{in}}$ is the largest contributor. However, the term J_1 amounts to about 20% of the total value and can definitely not be neglected. The last term, J_2, on the other hand, is only about 0.1% of the total value and can be discarded for the present case.

In reality the fracture energy, J_c, might not be constant during crack growth. When the adhesive layer starts to fracture, the conditions at the crack tip are altered. The presence of a more or less sharp crack can change the energy needed to fracture the adhesive layer (cf. Andersson and Stigh, 2003). For the present adhesive, experiments indicate that the fracture energy decreases as the crack propagates, cf. Section 6 and Fig. 9.

In order to provide a physical understanding of the fact that additional terms, besides J_0, are needed to obtain a correct value of J, the stress distribution in the adherends is studied. The lower solid curve of Fig. 8 shows the distribution of maximum (longitudinal) normal stress in the adherends at the onset of non-linear deformation (for the sawtooth model). The dotted line shows the beam theory prediction for the case of a

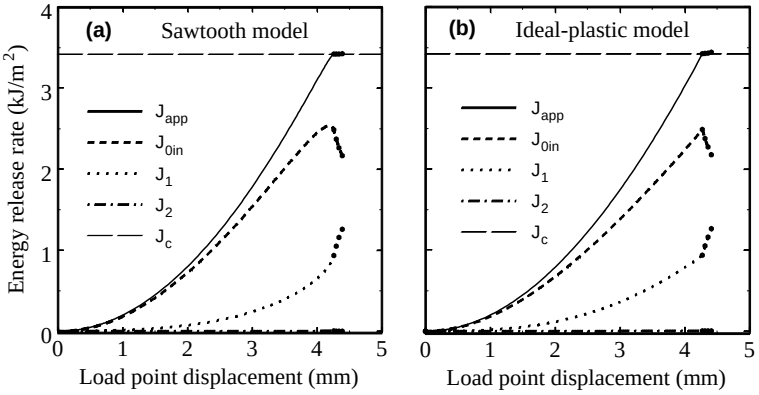

Fig. 7. The different terms in J_{app} according to Eq. (36). (a) Sawtooth model. (b) Ideal-plastic model. Dots indicate length of crack in 10 mm intervals (350, 360, 370, 380 mm). Initial crack length: 350 mm.

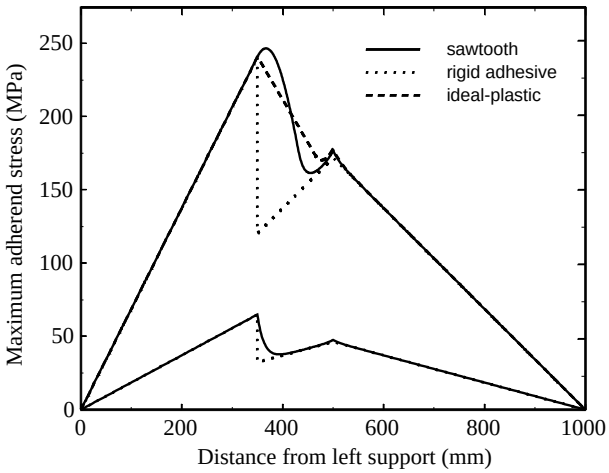

Fig. 8. Distribution of maximum normal longitudinal stress in adherends. Lower set of curves show situation at onset of non-linear deformation. Upper set of curves show situation at onset of crack propagation. Initial crack length: $a = 350$ mm.

rigid adhesive layer. This distribution obviously has a discontinuity at the crack tip due to the discontinuity of the bending resistance. This is an un-physical feature which is not present when the adherends are treated as individual beams connected by the flexible adhesive layer. This difference is the physical explanation to the presence of the additional terms in J, cf. Eq. (36), since the energy release rate essentially measures the elastic energy released by the adherends for a unit increase of the crack length. The upper curves of Fig. 8 show the distribution of maximum normal stress in the adherends at the onset of crack growth. The solid and dashed lines correspond to the sawtooth and the ideal-plastic model, respectively. The dotted line shows the beam theory prediction of the stress distribution for the case of a rigid adhesive layer. Also here, the difference between the present analysis and the results for a rigid adhesive layer can be noted. The difference is even more accentuated than it is at the onset of non-linear deformation, cf. the lower curves of Fig. 8. This indicates that the additional terms in Eq. (36) become more and more important as fracture is approached.

6. Experimental results

Results from experiments performed on a toughened epoxy adhesive and the geometry in Fig. 1 are presented here. The experiments are performed using a servo-hydraulic testing machine (MTS322). The displacement of the loading point is increased with a constant velocity of 1 mm/min. Both the applied force and the adhesive crack tip shear deformation are measured during a test. The force is measured with a load cell located between the actuator and the hydraulic grip. The shear deformation is measured using an extensometer (MTS632.03F-30). The resolution of the shear measurements is 0.05 μm. In order to minimize the friction between the adherends, PTFE-film is positioned inside the initial crack. For more information on details of the experiments, the reader is referred to Alfredsson et al. (2003).

In order to be able to evaluate the last term, J_2, in the approximate formula (36), the initial stiffness, k, must be known. In the previous simulations, it is assumed that the adhesive is linearly elastic up to a finite value of the deformation, cf. v_a or v_b in Fig. 4. For a real adhesive this might not be the case, i.e. the slope $\tau'(v)$ may change continuously in the elastic region. However, since the shear stress close to the loading point is small as compared to the maximum value of $\tau(v)$, the initial stiffness $k = \tau'(0)$ may be used.

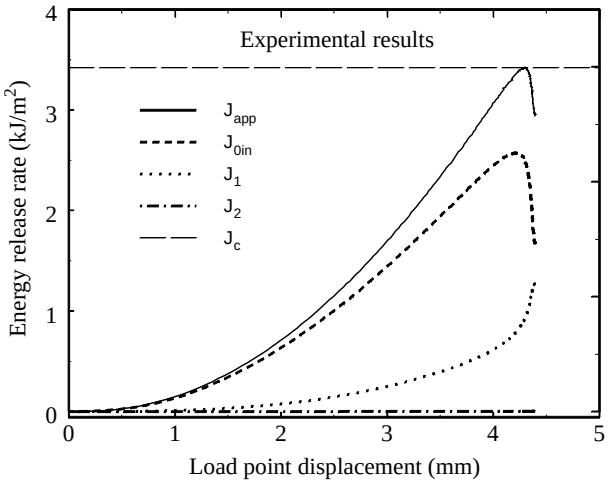

Fig. 9. The different terms in J_{app} according to Eq. (36). Experimental results.

Alfredsson et al. (2003) describe a procedure to determine the initial adhesive stiffness from data of the initial stage of an experiment. The procedure is based on the fact that, for small loads, the applied load, represented by $\bar{\tau}$, and the crack tip deformation, $v(0)$, are linearly related through Eq. (31a).

The evolution of the energy release rate during a test is obtained by inserting the measured values of P and v_{in} into Eq. (36). The result is shown in Fig. 9. The contribution from the different terms in Eq. (36) are also depicted in the figure. It is seen that the relative magnitudes of these terms correspond well to the results of the simplified models used in the simulations, cf. Fig. 7. Thus, for the present test geometry the two first terms, J_{0in} and J_1, dominate. The fact that the last term, J_2, is negligibly small means that the determination of the initial stiffness, k, is not crucial to the result. It is sufficient to obtain an approximate value of k. One may use $k = G/t$, where G is the shear modulus and t the thickness of the adhesive layer, respectively. The energy release rate has a maximum close to the end of the curve. Crack growth is assumed to occur at this maximum. Thus, J decreases beyond fracture, i.e. the fracture energy decreases as the crack propagates. As mentioned previously, this is attributed to changed conditions at the crack tip.

In Fig. 10a the values of the force, P, recorded during the experiment are shown as a function of the load point displacement, Δ. The agreement with the analytical solutions presented previously is fairly good. The initial non-linearity of the experimental result is due to initially poor contact at the loading point. The experimental results also show a more accentuated negative slope during crack growth, i.e. at the end of the curve. This is attributed to the fact that the fracture energy decreases during crack growth, a feature not included in the simulations. Fig. 10b shows the variation of the shear deformation at the crack tip. The agreement with the analytical solutions is good, especially the agreement with the "sawtooth model".

7. Stability of the ENF-specimen

It is well known that the ENF-specimen is only conditionally stable even for the case of a prescribed displacement of the loading point. Carlsson et al. (1986) investigated the stability for the case of a rigid adhesive layer. They found that stable crack growth takes place provided that the initial crack length is larger than the critical value,

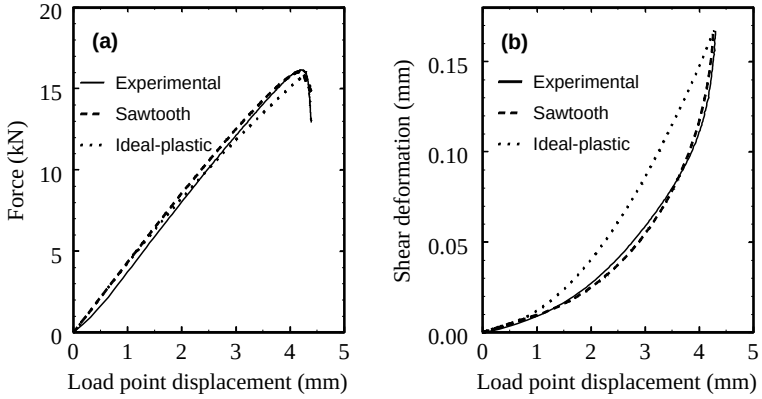

Fig. 10. (a) Progress of force P. (b) Progress of adhesive shear deformation at the initial crack tip. Comparison with analytical solutions.

$$a_{0,\mathrm{cr}} = \frac{L}{2 \cdot 3^{1/3}} \simeq 0.35L \tag{37}$$

A similar formula for the case with an arbitrary loading point is derived by Chai and Mall (1988). For the present configuration the value $a_{0,\mathrm{cr}} = 347$ mm is obtained.

The stability for the case of a compliant adhesive layer is studied next. In order to do this the deflection must be determined. Since the bending moment along the specimen is known, cf. Eq. (16), this is achieved from integration of Eq. (5b). For small loads, where the adhesive behaves linearly, the specimen is divided into three intervals containing a total of six new integration constants determined from the boundary conditions $w(-a) = w(c) = 0$ and the requirements of continuity of the deflection w and the slope w'. For higher loads, where the adhesive layer behaves non-linearly, the process zone gives an additional interval. Thus, four intervals containing eight integration constants are required. This procedure gives the deflection, $w(x)$, and the displacement of the loading point is given by $\Delta = w(b)$.

The resulting load–displacement curves are shown in Fig. 11 for three choices of initial crack length and the two different $\tau(v)$-curves, cf. Fig. 4. For a specific adhesive model, all curves coalesce for large values of the displacement. This is natural since the present model, for a specific value of the crack length, does not

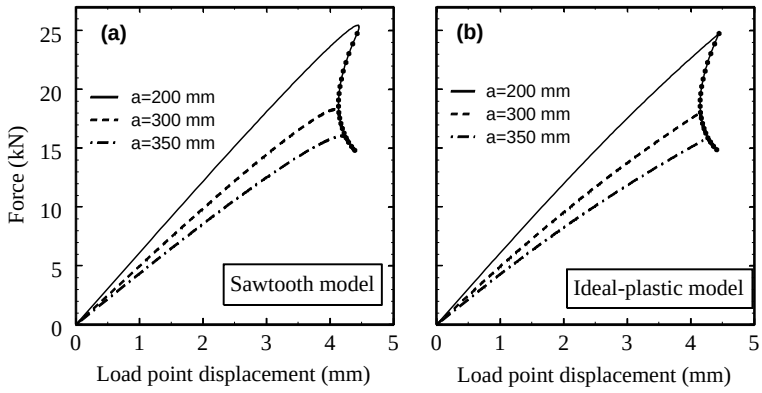

Fig. 11. Load–displacement paths for three values of initial crack length. (a) Sawtooth model. (b) Ideal-plastic model. Dots indicate start of crack growth with initial crack length in 10 mm intervals (200, 210, ..., 370, 380 mm).

distinguish if a crack has grown to the specific position or if this is the initial crack length at the onset of crack propagation. The dots on the curves of Fig. 11 indicate the points of start of crack growth for different values of the initial crack length ($a = 200, 210, \ldots, 370, 380$ mm). Alternatively, the dots can be seen as indicating different crack lengths during crack growth. The uppermost curve shows that for the shortest choice of crack length ($a = 200$ mm) the load–displacement path is unstable. The lowermost curve ($a = 350$ mm) corresponds to the geometry used in the experiments. This choice clearly gives a stable path, although the initial crack length is close to $a_{0,\mathrm{cr}}$ given by Eq. (37). Thus, the stability limit of Carlsson et al. (1986) is conservative. The actual stability limit of the present geometry is obtained for an intermediate choice of crack length. For both the sawtooth and the ideal-plastic model a critical crack length of about 285 mm is obtained, i.e. about 18% lower than $a_{0,\mathrm{cr}}$. The remainder of this section is devoted to developing an estimate of the critical crack length accounting for the presence of the adhesive layer.

From Fig. 11 it is obvious that stable crack growth is obtained for crack lengths giving negative slope in the $P(\Delta)$-curve. The present experiments are performed using a testing machine with a high stiffness. For situations where this is not the case, the stability limit is affected by the limited stiffness. If the compliance of the testing machine, C_{m}, is taken into account, the stability condition reads

$$\frac{\mathrm{d}\Delta}{\mathrm{d}P} + C_{\mathrm{m}} \leqslant 0 \tag{38}$$

For a *linear elastic adhesive*, the compliance, $\mathrm{d}\Delta/\mathrm{d}P = \Delta/P$, of the ENF-specimen, is approximately given by

$$C(a) = \frac{1}{32EWH^3}\left[12a^3 + L^3 + 36\left(\frac{a}{\kappa^2} + \frac{a^2}{\kappa} + \frac{L}{\kappa^2}\right) - \frac{72}{\kappa^3}\right] \tag{39}$$

where the same assumptions as in Eq. (31) are used. Equation (39) is a very good approximation as long as $\kappa b \geqslant 5$. During crack growth, the energy release rate equals the fracture energy, i.e. $J_{\mathrm{lin}} = J_{\mathrm{c}}$. Using Eq. (32), the crack length is expressed as a function of the load,

$$a = \frac{4}{3}\frac{W}{P}\sqrt{EJ_{\mathrm{c}}H^3} - \frac{1}{\kappa} \tag{40}$$

Inserting a from Eq. (40) into Eq. (39), and using the stability condition (38), leads to an algebraic equation in P. Using Eq. (40) again, an algebraic equation in a follows. The real root of this equation gives the critical value of the crack length,

$$a_{\mathrm{lin,cr}} = \frac{L}{2\cdot 3^{1/3}}\left(1 + \frac{36}{\kappa^2 L^2} - \frac{84}{\kappa^3 L^3} + 32\frac{EWH^3 C_{\mathrm{m}}}{L^3}\right)^{1/3} - \frac{1}{\kappa} \tag{41}$$

It can be noted that Eq. (37) giving the critical crack length for the case of a rigid adhesive layer, $a_{0,\mathrm{cr}}$, is regained from Eq. (41) with $C_{\mathrm{m}} = 0$ and $\kappa \to \infty$. For the present geometry $a_{\mathrm{lin,cr}} = 334$ mm, i.e. 4% lower than $a_{0,\mathrm{cr}}$. Thus, by accounting for the presence of the linear elastic adhesive layer a less severe condition follows. Numerical simulations for linear elastic adhesives show excellent agreement with Eq. (41). Thus, for brittle adhesives, Eq. (41) should provide a good estimate of the critical crack length. However, for more ductile adhesives it is still a too severe condition. Hence, the stability for ductile adhesives is studied next.

The most straightforward method to determine the stability limit for a *non-linear adhesive* is to examine the graphs in Fig. 11. This means, however, that the calculations outlined in Section 4 must be performed. Here, a simplified method to obtain an estimate of the critical crack length, is proposed. The method requires knowledge, or at least good approximations, of the fracture energy, J_{c}, and the critical shear deformation, v_{c}. It is utilized that, during crack growth, $J_{\mathrm{app}} = J_{\mathrm{c}}$ and $v(0) = v_{\mathrm{c}}$. The relation connecting the load and the crack length during crack growth is found using Eq. (33). Thus, during crack growth, the crack length is a function of the load,

$$a = \frac{4}{3}\frac{W}{P}\sqrt{EH^3}\left(J_c - \frac{3}{8}\frac{P v_c}{WH}\right)^{1/2} \tag{42}$$

where the last term in Eq. (33), i.e. J_2 in Eq. (36), is neglected. The deflection is approximately taken as for an ENF-specimen with a rigid adhesive, cf. Eq. (39),

$$\Delta = \frac{1}{32}\frac{P}{EWH^3}\left(12a^3 + L^3\right) \tag{43}$$

The deflection during crack growth is thus found as a function of the load by inserting a according to Eq. (42) into Eq. (43). Use of the stability condition (38) yields an algebraic equation in P. Using Eq. (42), an algebraic equation in a follows,

$$\frac{18a^3B(a)}{B(a) + 8a^2J_c} - 12a^3 - L^3 - 32EWH^3C_m = 0 \tag{44a}$$

where

$$B(a) = v_c\sqrt{EHD(a)} - D(a), \quad D(a) = v_c^2EH + 16a^2J_c \tag{44b,c}$$

Numerical solution of Eq. (44) yields a value of the critical crack length. For the present geometry, this gives an estimated critical crack length of 316 mm, i.e. 9% lower than $a_{0,cr}$. It is noted that this estimate is conservative as compared to the value 285 mm obtained by the more detailed analyses using the constitutive models shown in Fig. 4.

8. Conclusions and discussion

In the present paper a formula for the energy release rate of the ENF-specimen is derived. The derived formula for J, Eq. (36), consists of three terms. The first term is identical to the energy release rate for the case of a rigid adhesive layer. For the present case this term amounts to about 80% of the total energy release rate. The second term is proportional to the product of the applied load and the adhesive shear deformation at the crack tip. This term amounts to about 20% of the total energy release rate. The third term involves the elastic properties of the adhesive layer and is only about 0.1% for the present case. Equation (36) is an approximation which is shown to give excellent agreement for simulated experiments. Unlike previously presented formulas, the present one includes the effects of a flexible adhesive layer in an integrated manner. The actual shape of the stress-deformation relation need not be known. According to the formula, the applied load and the crack tip shear deformation must be measured in order to obtain a correct value of the energy release rate. On one hand, it is disappointing having to measure the crack tip shear deformation. On the other hand, the closed form formula (36) is an important improvement as compared to existing methods to estimate the energy release rate. Hence, it is the unpleasant truth that the crack tip shear deformation must be measured in order to obtain accurate values of J. Equation (36) gives a very good approximation of the instantaneous energy release rate as long as the adhesive shear deformation at the loading point is negligible as compared to the shear deformation at the crack tip. Technically, a small shear deformation at the loading point is achieved by making the distance, b, between the crack tip and the loading point large enough. For a linear elastic adhesive, the condition is $\kappa b \geqslant 5$. For the present non-linear adhesive, the approximate formula (36) gives good accuracy of the fracture energy, J_c, provided that $\kappa b \geqslant 10$. In order to be able to study a possible change of the fracture energy during crack growth, the condition $\kappa b \geqslant 10$ can still be used, if b is taken as the value at the end of crack growth.

The improved approximate formula (36) for the energy release rate of the ENF-specimen, extends the applicability to situations where the adhesive is ductile. As shown, cf. Fig. 9, the correction term can be

quite large, in this case more than 20% of the total value. For the present geometry, the maximum adherend stress is approximately half the yield strength, cf. Fig. 8. Thus, it is possible to use adherends with a smaller height without jeopardizing the requirement that the adherends must deform elastically. Alfredsson et al. (2003) present a technique for design of the ENF-specimen, using the fixed ratio $a/L = 0.35$ in order to ensure stability. For the present adhesive with a fracture energy of 3.42 kJ/m^2 and a critical deformation of 0.167 mm, it is found that with a yield strength of the adherend material of 500 MPa, the smallest possible adherend height is $H = 10$ mm. This value is only weakly dependent on the specimen length. With the same specimen length as in the present paper ($L = 1000$ mm), the relative size of the correction term decreases slightly ($J_{0\text{in}}/J = 0.85, J_1/J = 0.15$). However, with $H = 10$ mm, the load point displacement at fracture ($\Delta_c = 25$ mm) is larger than the total height of the specimen. In order not to introduce non-linear geometrical effects, that may jeopardize the validity of the formula, the larger adherend height $H = 32$ mm is chosen. Thus, it is found that large specimens are necessary to give reliable data for a tough engineering adhesive. It would theoretically be possible, by using a very long specimen, to make all terms in Eq. (36) except $J_{0\text{in}}$ negligible, and thus avoid the necessity to measure the adhesive shear deformation at the crack tip. By for example choosing the smallest possible adherend height, $H = 10$ mm, and $L = 5000$ mm, $J_{0\text{in}}$ is responsible for about 97 % of the total J. However, such a long specimen cannot be handled in practice, not mentioning that the load point displacement is several hundred mm:s for this case.

For the particular experiment presented in this paper the fracture is cohesive, i.e. it takes place inside the adhesive. Thus, microcracks and voids are formed in the interior of the adhesive layer, eventually leading to macroscopic fracture of the adhesive layer. However, the method can handle also situations where the fracture is adhesive, i.e. crack growth takes place at the adherend/adhesive interface. This is understood by studying the definition of J, cf. Eq. (18), and noting that the arbitrary constitutive relation, $\tau(v)$, is a relation between the stress acting at the adherend/adhesive interface and the *total* deformation of the adhesive *layer*. Thus, Eq. (36) gives the instantaneous energy release rate and finally the fracture energy, irrespective of the actual failure mechanism.

In the present paper it is presumed that the load is applied centrally between the supports. Thus, the level of shear deformation to the right of the loading point is relatively small. From Fig. 6 it might appear as if this part of the specimen is inactive. In order to reduce the size of the specimen it might thus be tempting to reduce the size of this ''inactive'' part by applying the load non-centrally, i.e. closer to the right support. However, numerical simulations show that the shear deformation at the loading point is non-zero for the linear elastic case even when no crack is present. Moreover, for the linear elastic case, the position where the shear deformation is zero depends on the size of the crack. Thus, for the general case with an unknown non-linear constitutive relation, it is not possible to estimate the accuracy of an approximate formula similar to the one in Eq. (36), if the load is applied non-centrally.

Equations (29) and (30) serve as powerful tools to estimate the length of the process zone. For the present case, the sawtooth model gives a smaller process zone (81 mm) as compared to the ideal-plastic model (115 mm), cf. Fig. 6a. Simulations with other adhesive data, indicate that this is a rather general result. However, the difference is not that large, considering that the two models are fundamentally different. The size of the process zone is quite large, about three times the adherend height and several hundred times the adhesive thickness ($t = 0.2$ mm), for the present geometry. Large process zones (as compared to the adhesive thickness) is common with adhesive layers (e.g. Hunston et al., 1989; Chai, 1993). This seems to be a result of the ductility of the adhesive. Even with the smallest possible adherend height ($H = 10$ mm, $L = 1000$ mm) the process zone is large, about 50 mm. With a fixed value of H the size of the process zone is only slightly affected by the length of the specimen. If L is made smaller, the size of the process zone increases somewhat, and vice versa.

The critical crack length for stable crack growth is here, and by Carlsson et al. (1986) and Chai and Mall (1988), estimated using the assumption that the fracture energy is constant during crack growth. For the present case, where the fracture energy decreases as the crack propagates, fracture might be stable at first

and later turn unstable. Thus, in practice it might be preferable to use the conservative value of the critical crack length provided by Eq. (37). It would, however, be possible to investigate the effect of a decreasing fracture energy on the critical crack length, by use of Eq. (44).

Acknowledgements

The work presented in this paper is part of a co-operation project with the group of Mechanics of Materials and Computational Solid Mechanics at the Department of Applied Mechanics, Chalmers University of Technology, Göteborg, Sweden. The author would like to thank Prof. Ulf Stigh at the Department of Engineering Science, University of Skövde, Sweden, for helpful comments and discussions.

References

Alfredsson, K.S., 2003. On the determination of constitutive properties of adhesive layers loaded in shear—an inverse solution. International Journal of Fracture 123, 49–62.

Alfredsson, K.S., Biel, A., Leffler, K., 2003. An experimental method to determine the complete stress-deformation relation for a structural adhesive layer loaded in shear. In: Proceedings of the 9th International Conference on the Mechanical Behaviour of Materials.

Andersson, T., Stigh, U., 2003. The stress-elongation relation for an adhesive layer loaded in peel using equilibrium of energetic forces. International Journal of Solids and Structures 41, 413–434.

Barrett, J.D., Foschi, R.O., 1977. Mode II stress-intensity factors for cracked wood beams. Engineering Fracture Mechanics 9, 371–378.

Beer, F.P., Johnston, E.R., DeWolf, J.T., 2002. Mechanics of Materials, third ed. McGraw-Hill, New York.

Carlsson, L.A., Gillespie, J.W., Pipes, R.B., 1986. On the analysis and design of the end notched flexure (ENF) specimen for mode II testing. Journal of Composite Materials 20, 594–604.

Chai, H., 1988. Shear fracture. International Journal of Fracture 37, 137–157.

Chai, H., 1993. Observation of deformation at the tip of cracks in adhesive bonds loaded in shear and assessment of a criterion for fracture. International Journal of Fracture 60, 311–326.

Chai, H., Mall, S., 1988. Design aspects of the end-notch adhesive joint specimen. International Journal of Fracture 36, R3–R8.

Chatterjee, S.N., 1991. Analysis of test specimens for interlaminar mode II fracture toughness, Part 2. Effects of adhesive layers and material nonlinearities. Journal of Composite Materials 25, 494–511.

Corleto, C.R., Hogan, H.A., 1995. Energy-release rates for the ENF specimen using a beam on an elastic-foundation. Journal of Composite Materials 29 (11), 1420–1436.

Ding, W., Kortschot, M.T., 1999. A simplified beam analysis of the end notched flexure mode II delamination specimen. Composite Structures 45, 271–278.

Hunston, D.L., Kinloch, A.J., Wang, S.S., 1989. Micromechanics of fracture in structural adhesive bonds. Journal of Adhesion 28, 103–114.

Klarbring, A., 1991. Derivation of a model of adhesively bonded joints by the asymptotic expansion method. International Journal of Engineering Science 29, 493–512.

Mi, Y., Crisfield, M.A., Davies, G.A.O., Hellweg, H.-B., 1998. Progressive delamination using interface elements. Journal of Composite Materials 32, 1246–1272.

Olsson, P., Stigh, U., 1989. On the determination of the constitutive properties of thin interphase layers—an exact inverse solution. International Journal of Fracture 41, R71–R76.

Russel, A.J., Street, K.N., 1982. Factors affecting the interlaminar fracture energy of graphite/epoxy laminates. Progress in Science and Engineering of Composites (ICCM-IV), Tokyo, 279–286.

Salomonsson, K., 2002. Interphase elements connecting structural finite elements—formulation, implementation and verification. Masters Thesis, Chalmers University of Technology, Göteborg, Sweden.

Schmidt, P., 2001. Analysis of adhesively bonded joints—an asymptotic approach. Linköping Studies in Science and Technology, Thesis No. 925, Linköping University, Linköping, Sweden.

Sørensen, B.F., 2002. Cohesive law and notch sensitivity of adhesive joints. Acta Materialia 50, 1053–1061.

Stigh, U., 1988. Damage and crack growth analysis of the double cantilever beam specimen. International Journal of Fracture 37, R13–R18.

Stigh, U., Andersson, T., 2000. An experimental method to determine the complete stress–elongation relation for a structural adhesive layer loaded in peel. In: G.J. Williams (Ed.), Proceedings of the 2nd ESIS TC4 Conference on Polymers and Composites, Les Diablerets, Switzerland, pp. 297–306.

Ungsuwarungsri, T., Knauss, W.G., 1987. The role of damage-softened material behaviour in the fracture of composites and adhesives. International Journal of Fracture 35, 221–241.

Wernersson, H., Gustafsson, P.J., 1987. The complete stress-slip curve of wood adhesives in pure shear. In: Verchery, G., Cardon, A.H. (Eds.), Mechanical Behaviour of Adhesive Joints. Edition Pluralis, Paris, pp. 139–150.

Xia, Z.C., Hutchinson, J.W., 1994. Mode II fracture of a brittle adhesive layer. International Journal of Solids and Structures 31 (8), 1133–1148.

Zou, Z., Reid, S.R., Li, S., 2003. A continuum damage model for delaminations in laminated composites. Journal of the Mechanics and Physics of Solids 51, 333–356.